Bulletin of the New Zealand Society for Earthquake Engineering, Vol. 55, No. 2, June 2022

COMPARISON OF NONLINEAR RESPONSE OF GRAVITY CANTILEVER RETAINING WALLS AND MECHANICALLY STABILISED EARTH (MSE) WALL STRUCTURES

Arman Kamalzadeh[1] and Michael Pender[2]

(Submitted *March 2021*; Reviewed *June 2021*; Accepted *March 2022*)

ABSTRACT

During the past few decades, gravity cantilever retaining walls (GRW) have shown a relatively reliable performance. However, mechanically stabilised earth (MSE) retention systems have grown in popularity as they are cost-effective and have demonstrated resilience through recent seismic events. In this study, utilising 2D finite element (FE) modelling with OpenSees and the Manzari and Dafalias constitutive models, we have compared the seismic behaviour of GRW and MSE systems, both designed for the same conditions, under three earthquake records. These earthquake excitations were recorded on engineering bedrock (V_s > 700 m/s) to avoid complexities of deconvolution. Our investigations indicate that the retained MSE reinforced soil block behaves similarly to a rigid block, while this is not the case for the soil over the foundation heel in the GRW system. In addition, the lateral displacement over the height of the wall for MSE is at about half that of a GRW. In the final section of this paper, we discuss the effect of backfill compaction. It is shown that regardless of the retention system, the backfill density increasing from medium (D_r = 70%) to dense (D_r = 100%) reduces the lateral displacements by at least 50%.

INTRODUCTION

Retaining structures have brought sustainability to our societies by securing buildings and infrastructure such as bridge abutments, highways, offshore structures, etc. The original retaining structures were masonry gravity walls, maintaining the stability of the backfill with their weight, but they may not be economical as they require a large amount of material. For this reason, reinforced concrete cantilever retaining walls gained popularity as they substituted the mass of masonry or concrete by backfill above the heel of the footing. Well-designed and constructed gravity retaining walls (referred to GRW in this study) of modest height generally resist mild seismic events without damage, even though they may only have been designed for gravity loading [1,2]. Preventing the failure of the wall-foundation system due to severe earthquake damage can often lead to a costly design. Richards and Elms [3] and the NZTA bridge manual [4] proposed the acceptance of limited permanent lateral displacement to reduce the wall forces, hence reducing wall dimensions and costs. However, even with allowing permanent displacements in the design of gravity cantilevered walls, other wall systems can be more cost effective.

On the other hand, an alternate solution for retaining slopes and backfill has emerged during the past few years. Mechanically Stabilised Earth (MSE) structures, using segmental concrete facing blocks and steel strips/geogrid reinforcement, are a viable solution with reduced cost, ease and speed of construction, and differential settlement tolerance [5-8]. MSE walls have shown encouraging resiliency during major seismic events such as the 2011 Tohoku earthquake. Upon inspection after this Richter magnitude 9.0 event in an area that the seismic demand surpassed the design level, 90% of the 1600 MSE walls remained unharmed while only 1% were severely damaged [9].

Transfund guidelines endorsed by the New Zealand Transport Agency (NZTA) [10] has categorised the failure mechanisms of MSE retaining walls into external (sliding, overturning, bearing capacity and, deep-seated) and internal (reinforcement pullout and rupture, and sliding between the layers). Although the discussion on the dominant failure mechanism is not as agreed upon as that for gravity cantilevered retaining walls, several researchers have reported an external failure mechanism for even a well designed and constructed MSE wall [11-14].

This study compares the seismic response of cantilever and MSE walls of corresponding heights with various underlying and backfill soil relative densities under the same dynamic excitations. For this comparison, we used the OpenSees finite element software [15] and used the Manzari-Dafalias (MD) constitutive relationship [16], a two-surface plasticity model with a non-associative flow rule.

METHODS OF STUDY

Finite Element Modelling

The finite element (FE) modelling is executed using OpenSees 3.1.0 [15]. These simulations are in a 2D plane strain environment. GiD [17], a pre/post-processing software, is also implemented to build the geometry of the soil-wall interaction and processing results.

Constitutive Model

Lee and Seed [18], in 1967, based on a series of drained triaxial experiments on Sacramento River sand, reported that medium to dense sands experience a peak shear strength before reaching their ultimate strength. To this date, constitutive models capable of modelling the full range of shearing behaviour of loose to dense sand are scarce. However, Dafalias and Manzari [16] proposed a constitutive model capable of capturing this peak shear strength by implementing a two-surface plasticity approach with a non-associative flow rule. This constitutive model is coded in the OpenSees material library as Manzari-

[1] *Corresponding Member, PhD Student, Department of Civil Engineering, University of Auckland, akam553@aucklanduni.ac.nz*
[2] *Professor Emeritus, Department of Civil Engineering, University of Auckland, (Life Member)*

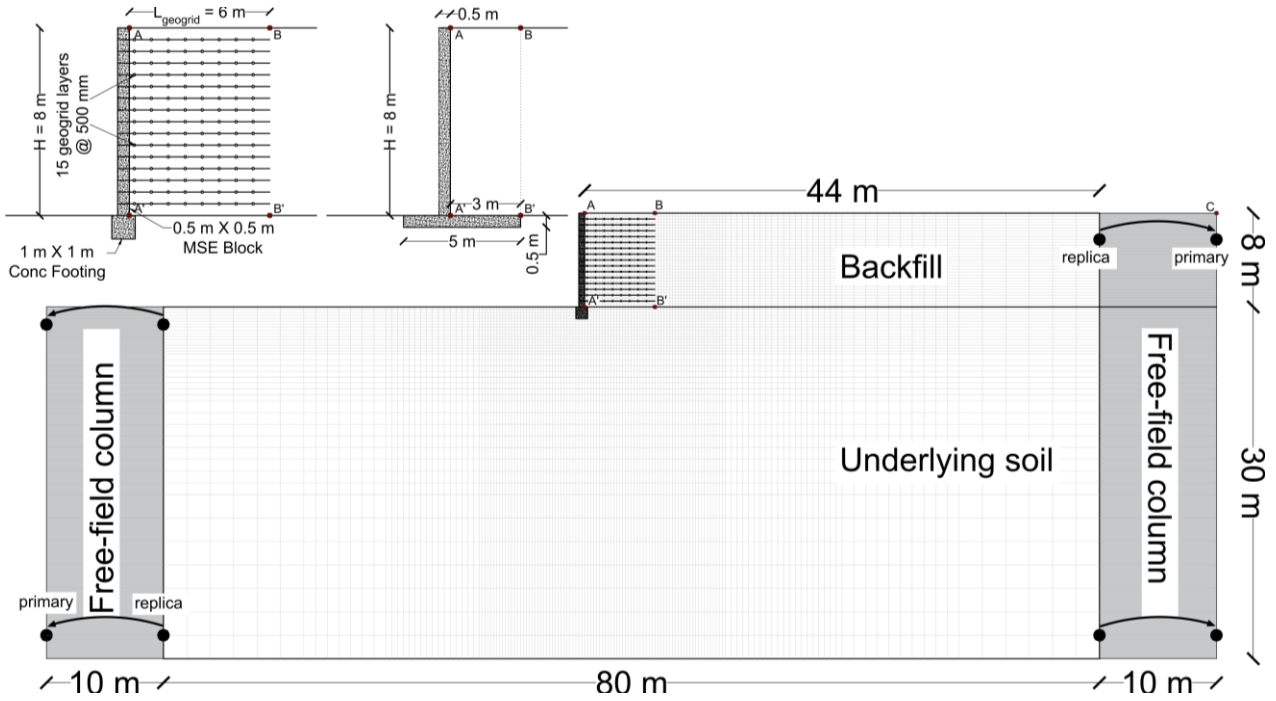

Figure 1: Geometry and retention system.

Dafalias (MD) [19]. Several studies have found that the MD model (or a similar version) leads to a reasonable granular soil representation [20-23]. This study has adopted the calibrated input parameters for Toyoura sand [16, 24].

Wall Systems

The reinforced concrete and blocks of gravity cantilever and MSE walls are simulated using elastic isotropic material, with an elastic modulus and Poisson's ratio of 30GPa and 0.2, respectively. The geogrids of the MSE retention system are simulated with a tension-only elastoplastic link. The yield strength (T_y) and tensile stiffness (J) are assumed to be 157.3 and 2,000kN/m, respectively [8]. Note that these values are presented per unit of out-of-plane length. The block-block and soil-block interfaces are frictional and elastic-no tension in the tangential and axial directions, while the interface is only frictional for soil-geogrid. The soil-block and soil-geogrid interface friction angles are assumed 2/3 and 1.0 of the backfill friction angle, respectively. The equivalent friction angle of the backfill is derived from drained triaxial simulations. The block-block interface friction angle of 57° is derived from [25, 26]. If required, the initial values for the normal (k_n) and tangential (k_s) interface stiffness recommended in [25, 26] are altered in a trial-and-error process to achieve convergence.

Geometry

The underlying and backfill soil medium dimensions are 80m x 30m and 44m x 8m (see Figure 1). The mesh sizes are 250 and 100mm in the vicinity of the MSE and GRW wall, respectively. The mesh is smaller in and around the reinforced soil while getting larger towards the bottom corners of the soil medium. To reduce the computational workload while maintaining precision, single Gauss point quadrilateral elements have been deployed [27].

The MSE wall system contains a 1m x 1m concrete footing and 8m high concrete block facings, each with a dimension of 0.5m x 0.5m. There are 15 layers of geogrids vertically spaced at 500mm. The geogrid length follows the instruction of being longer than 70% of the wall height [2, 28], which is L = 6m in our case.

The gravity retaining wall dimensions are in line with the suggestions of Clayton et al. [29] and Pender [30]. The gravity cantilever retaining wall system has a stem of 8m and a foundation width of 5m with a 3m heel projection. Both the stem and foundation have a thickness of 500mm (note Figure 1 for details on MSE and gravity cantilever walls).

In Figure 1, points A and A' show the top and base of the wall stem and points B and B' indicate the top and bottom of the back end of the MSE block or the back end (virtual back) of GRW. These abbreviations have been used in subsequent figures.

Boundary Conditions

As shown in Figure 1, the model is contained by two 10m wide free-field soil columns on the sides. These columns hold the same properties as their neighbouring soil. However, they have a lateral extent (out of plane) of 1,000m, which is 1.0m for the inner soil model. The effect of this significant relative lateral extent is to increase the mass on both sides of the model, mimicking a situation where the inner model is part of a tremendously wide soil domain. At each specific elevation, the inner node (replica) is tied to the outer node (primary) of the free-field columns in both translational directions to enforce periodic boundary conditions (see Figure 1). The great mass of the free-field columns and the periodic boundary conditions impose the free-field response in the side columns [31-33]. This ensures 1D seismic wave propagation during seismic analyses. Note that the free-field column nodes are not fixed in any direction (excluding the nodes at the base).

During static analyses to allow in-situ conditions, the base of the model is fixed in both degrees of freedom (DOFs), while throughout dynamic analyses, it is only fixed in the vertical DOF. All of the nodes at the base (replicas) are tied to the bottom left corner node (primary) in the horizontal DOF to ensure uniform displacement at the base during excitation. The primary node at the bottom left corner is attached to a Lysmer and Kuhlemeyer [34] dashpot. The other end of the dashpot is fixed in both directions. This technique, known as the compliant base in some sources, could imitate the dissipation of dynamic waves through an engineering bedrock [35].

Analyses

Staged Construction

The model is sequentially constructed and analysed to match the actual staged construction process. First, the underlying soil is analysed to put in-situ conditions in place. Then the foundation of the wall is situated. Afterwards, the backfill soil layers, concrete blocks, geogrid layers (if applicable) and interfaces are simulated and analysed for each 500mm height. This last step is iterated until the wall reaches 8m in height. Following the complete construction, input excitation is applied, and the model is analysed with the proper boundary conditions.

Sinusoidal Waves

To determine the natural period of the soil medium in Figure 1, a series of ten-pulse sinusoidal excitations with various period values has been used. The period values range from 0.167s to 10s. By employing these excitations as input at the bottom of 1D soil columns, we could estimate the natural period of this 1D column for linear and nonlinear soil. The geometry and soil properties of these 1D soil columns are identical to the right side free-field soil column in Figure 1. Subsequently, while using the sinusoidal excitations with period values around the 1D soil column natural period, we compared the response of the linear 1D and 2D soil models.

Ground Motions

Almost all of the ground motions in the existing databases are recorded at the ground level. However, for soil-structure interaction analyses, one requires the excitation at the base of the model as the earthquake characteristics change as it travels through soil layers. Nonlinear deconvolution is a signal transformation process that estimates the ground motion signal at a certain depth before reaching the surface. For simplification, we have assumed our model in Figure 1 is contained by an outcrop at the sides and bottom. This assumption allows for the adoption of the suggestion of Kokusho and Sato [36]. They inferred that if an engineering bedrock confines a soft soil medium at the sides and the bottom, the recorded acceleration on the bedrock surface is double in magnitude at the bottom of the soil medium without the frequency content of the ground motion changing exceedingly. Therefore, in this study, three earthquake records from PEER NGA-West 2 database [37] on engineering bedrocks with V_s > 700m/s with no considerable near-fault pulses are employed. Table 1 summarises the seismic excitations used in this study.

Table 1: Ground motions characteristics.

Earthquake	Station	Magnitude (M_w)	V_s ($\frac{m}{s}$)	PGA (g)
Iwate (2008)	IWT010	6.9	826	0.22
Manjil (1990)	Abbar	7.37	724	0.55
ChiChi (1999)	HWA003	7.62	1526	0.14

Figure 2 illustrates the acceleration time histories of Table 1. Figure 3 shows the acceleration spectra of the seismic records in Table 1 scaled to PGA of 0.15g. As shown, the Manjil and Iwate spectra have higher accelerations at shorter periods, while the ChiChi could lead to higher responses in soil media with higher natural periods.

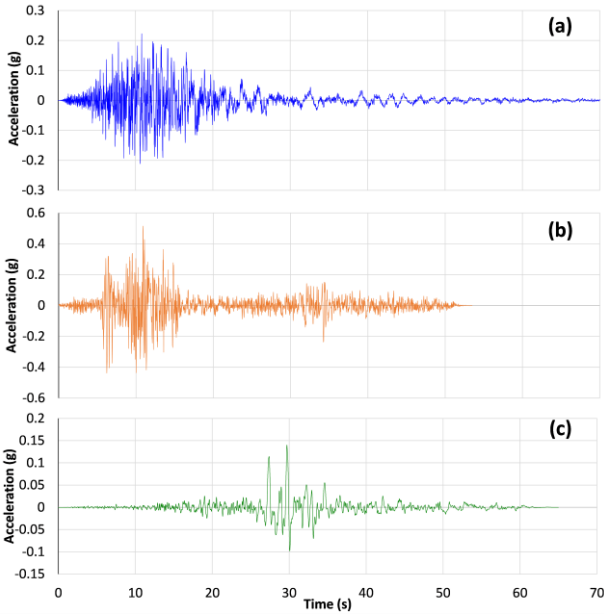

Figure 2: Acceleration time-histories for ground motions; a) Iwate, b) Manjil, and c) ChiChi.

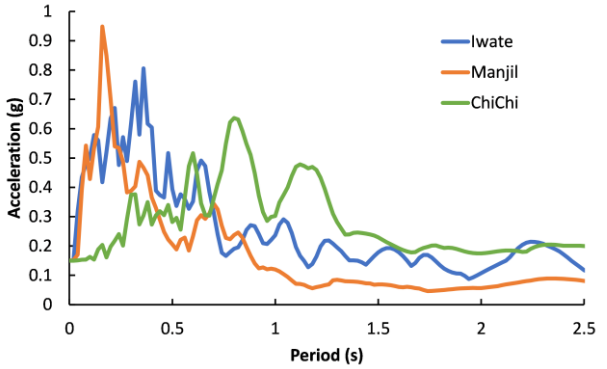

Figure 3: Acceleration spectra of input earthquakes with PGA values scaled to 0.15g.

DISCUSSION AND RESULTS

Fundamental Period Assessment

As explained in previous sections, sinusoidal excitations with various period values have been utilised to compare the responses of 1D and 2D soil models. Figure 4 shows the response spectra for 1D linear and nonlinear soil columns and 2D linear soil models at points A and C (see Figure 1). The acceleration response spectra of Figure 4 are normalised to the maximum input acceleration of 0.15g at the base of the model, i.e., indicating the spectral amplification of the input motion. The relative density of the founding and backfill soils are 70% and 100%, respectively. As observed, at a period of 1.1s, the maximum response acceleration would be around twelve times the maximum input acceleration for a linear 1D soil column. This magnification reduces to less than 4.0 at a corresponding period of 1.25s for a nonlinear 1D soil column. The reduction of the magnification value and the increase of the natural period is probably an indicator of internal damping due to nonlinearity in the soil body. Therefore, if the linear 1D site response amplification factor is used as a division factor for the ground motion time history for 2D or 3D nonlinear simulations, the acceleration at the top will be less, resulting in underestimation.

The conventional method ($T = 4H/V_s$) estimates 0.81s as the characteristic site period, considering the 38m deep soil column and average sheer wave velocity of 187.5m/s. This period is lower than both 1.1 and 1.25s, natural periods discussed above.

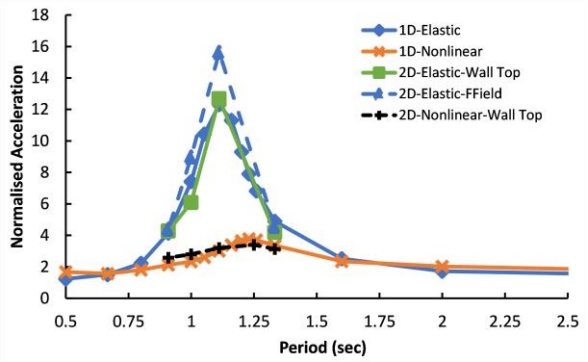

Figure 4: Response of 1D and 2D models to sinusoidal excitations.

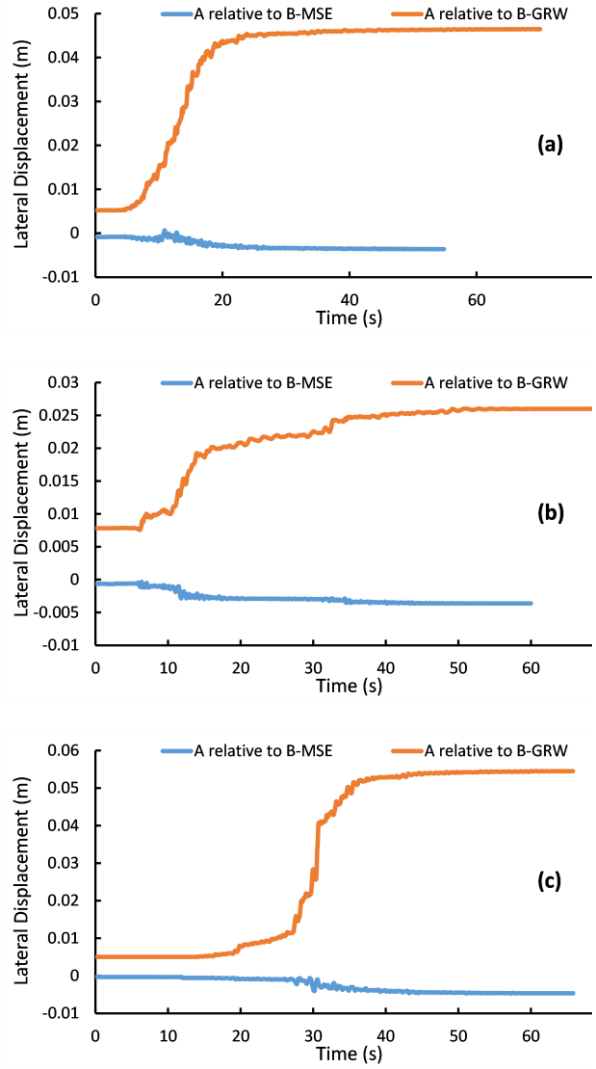

Figure 5: Wall top lateral displacement relative to the top of MSE block end/virtual back of cantilever wall when the founding and backfill soil D_r = 70% and 100% for earthquakes; a) Iwate, b) Manjil, and c) ChiChi.

Interestingly, the response of the nonlinear 2D soil model at the top of the wall is almost identical to the nonlinear 1D soil column; the same goes for linear models. This can imply that the free-field PGA is almost equal to the effective acceleration on the wall system and can be used for design purposes. According to these results and Figure 3, it is expected that the ChiChi motion will have the most significant impact on the wall system, while the Manjil motion will have the least.

MSE vs GRW Retention System

Figure 5 illustrates that the lateral displacement of the top of the wall facing relative to the top of the MSE block end is noticeably lower than cantilever retaining walls. Also, while the top of the cantilever wall moves outwards, this movement is slightly inwards for the MSE block.

Figure 6 illustrates the settlement profiles at the bottom and top of the walls. Note that the facing of the walls is at the length of zero in Figure 6. As Figure 6a indicates, the difference of settlement at the bottom of the walls is not high. However, the foundation of GRW tilts outward for the Iwate and ChiChi's ground motions while the base of the MSE system (excluding the 1m x 1m foundation block) rotates slightly inward. The settlement at the backfill surface is shown in Figure 6b. Within the geogrid extent of the MSE system, the settlement is 20% less than the GRW system. However, immediately outside the geogrid zone, the backfill surface experiences an abrupt 50% settlement increase, Bathurst et al. [38] also reported similar behaviour. This can be translated into increased horizontal stiffness in the MSE block due to geogrid application leading into a rigid movement of reinforced soil and differential lateral movement between the reinforced and unreinforced backfill. This is discussed more extensively in Figure 9a and Figure 11a. Although initially it was believed that geogrid layers would act in tension, this might indicate that the frictional interface between the geogrid layers and retained soil can increase confinement in the soil, hence the rise in the MSE block stiffness. In addition, this sudden drop in settlement can cause damage to any service lines behind the wall and should be considered when designing these structures.

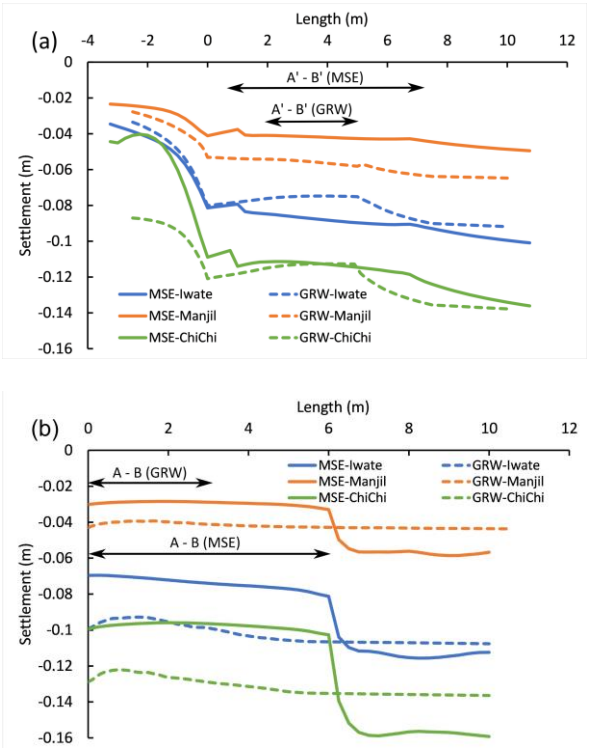

Figure 6: Settlement profiles when the founding and backfill soil D_r = 70% and 100% at a) bottom of the backfill level and b) top of the backfill level.

Figure 7a displays the lateral displacement distribution relative to the base of the wall (point A' in Figure 1) over the wall height. While the maximum displacement occurs at the top of GRW, MSE walls experience the maximum at a point lower than half the height of the wall. The GRW rotates outwards, but the MSE systems respond with a gentle bulge in the lower half. Therefore, despite the maximum displacement at the top for the cantilever type retaining walls, lower mid-height is the peak displacement occurrence for MSE walls. Also, the MSE wall lateral displacements are less by 40% for Manjil to the 85% for Iwate motion. Figure 7b illustrates the lateral displacement of line A-A' (wall front) to B-B' (back of the wall systems). As can be observed, there is almost no relative displacement between the front and back of the MSE wall over the height, meaning that the MSE behaves similarly to a rigid block. In contrast, for the GRW systems, a gap forms between the front and the back of the system, reaching its maximum value at the top.

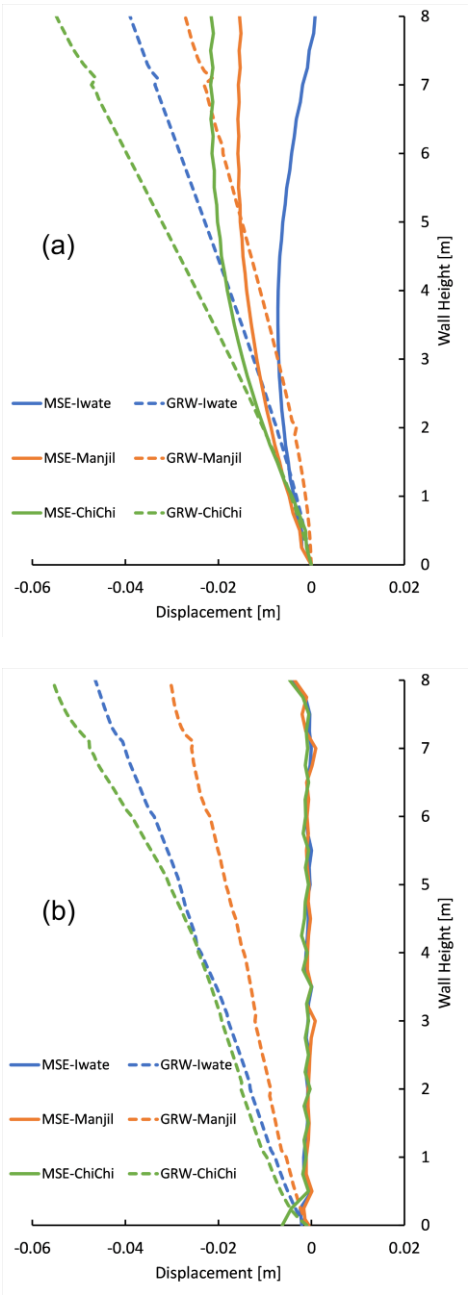

Figure 7: Lateral displacement distributions for cases Dr = 70% and 100% in the founding and backfill soils, respectively; a) relative to the base of the wall (A'), and b) A-A' relative to B-B'.

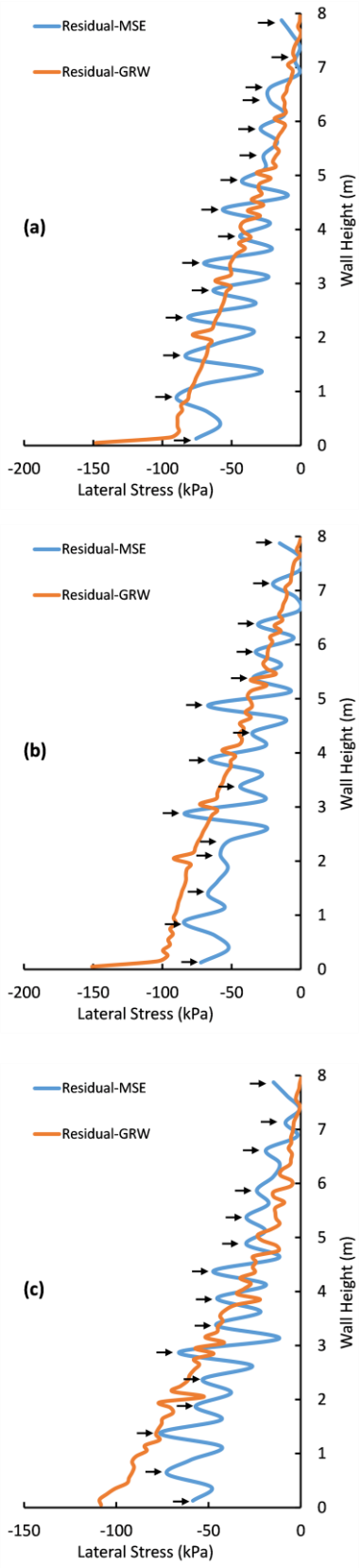

Figure 8: Residual lateral stress distribution over the end of MSE block/virtual back of cantilever wall (B-B') when the founding and backfill soil D_r = 70%, and 100%, respectively for earthquakes; a) Iwate, b) Manjil, and c) ChiChi.

Figure 8 compares the lateral earth pressures after seismic excitation (residual) at the back end of the GRW and MSE systems. As can be seen, there is little difference between the overall magnitude of lateral stresses over the back of the wall systems. One can observe that the residual lateral earth

pressures distribution for the MSE walls contains multiple fluctuations and is not smooth as expected. These fluctuations on the lateral stress distribution, pointed out by arrows on the Figure 8, have 15 spikes at the exact location of each geogrid layer. These spikes are probably a sign of lateral stiffness differences between the geogrid layers and surrounding soil.

Figure 9 illustrates the displacement vectors for both the MSE and GRW systems after the Iwate motion; both scaled identically. The orientation and length of these vectors show the direction and magnitude of soil nodal movements. Note that the concrete elements are removed from this figure. Figure 9a confirms previous results that the reinforced soil behaves as a rigid block that can indicate increased lateral stiffness due to geogrid layers. In Figure 9a, for any vertical line stretching from the bottom to the top of the backfill, inside and outside the reinforced block, the magnitude and orientation of the soil elements are almost identical, except for the red dashed area shown. This irregular area, with an approximate lateral extent and depth of 2.5 and 5m, respectively, can indicate a tensional crack behind the reinforced soil. This is also apparent in Figure 11a. On the other hand, Figure 9b shows significant movement inside and outside the GRW virtual block, especially towards the top left corner behind the wall stem. A similar pattern can be observed in Figure 11b.

The contours of lateral displacement for Iwate excitation are shown in Figure 10. In the case of the MSE system, the 6m wide block displaces almost as a rigid block. On the other hand, for the GRW system, the contours concentrate on areas towards the top of the wall, and there is little evidence that the soil body on top of the foundation heel acts as a rigid block.

While the MSE system pushes back the lateral strain demand at the back of the block, the maximum lateral strain for the GRW system extends from 3m below the top to 3m behind the wall at the backfill surface (see Figure 11). Furthermore, the GRW system seems to mobilise the passive resistance at the toe more than the base block of the MSE system. The MSE wall's behaviour indicates a global failure mechanism (deep-seated or tensional crack in this case), but an internal failure mechanism is evident between the GRW stem and the virtual back.

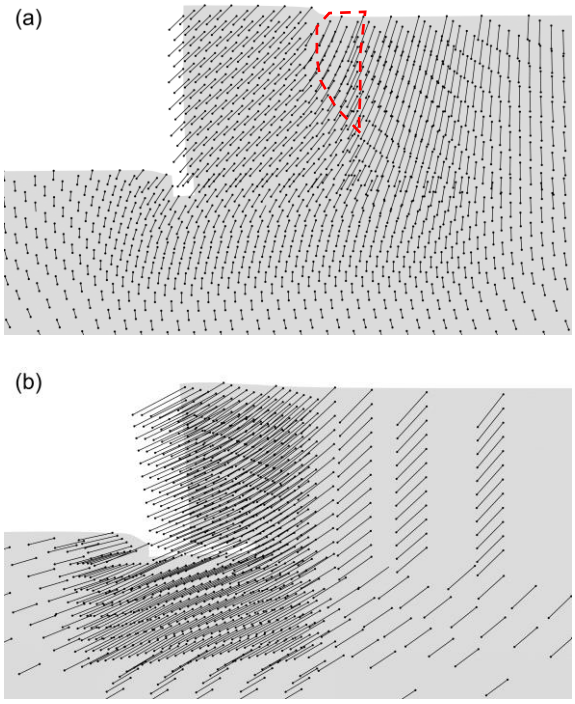

Figure 9: Displacement vectors on deformed shapes for D_r = 70% and 100% for founding and backfill soil, respectively, and Iwate excitation for; a) MSE and b) gravity wall.

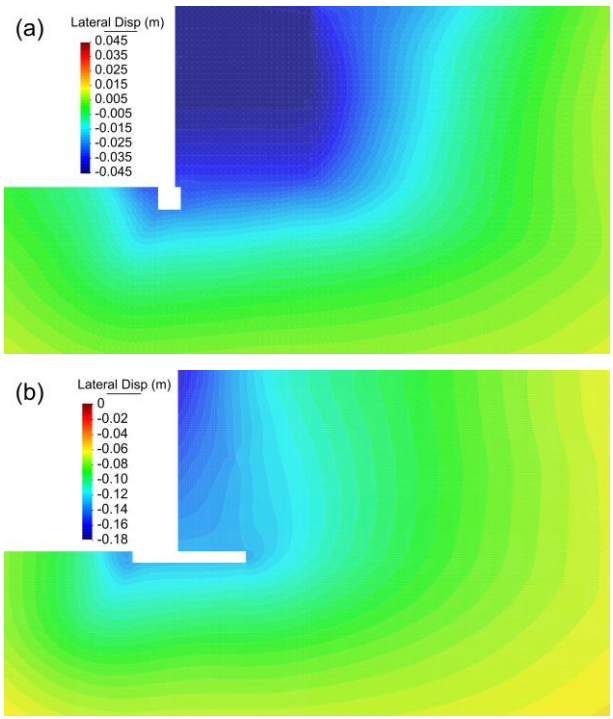

Figure 10: Lateral displacement contours for D_r = 70% and 100% for founding and backfill soil, respectively, and Iwate excitation for; a) MSE and b) gravity wall (note that the scales are different).

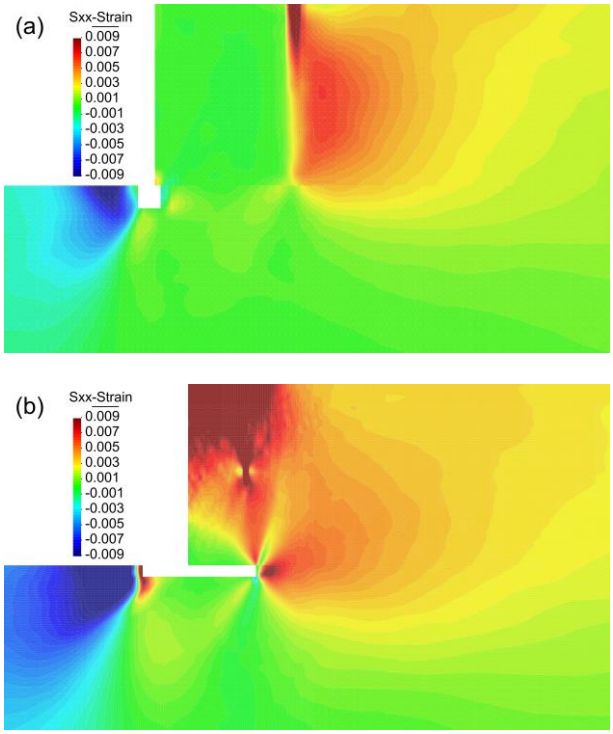

Figure 11: Lateral strain contours for D_r = 70% and 100% for founding and backfill soil, respectively, and Iwate excitation for; a) MSE and b) gravity wall.

Backfill Compaction

Figure 12 presents deformation comparisons between backfills with 70% and 100% relative densities for three cases; these relative densities can be approximately correlated to 95% and 100% compaction to the maximum dry density (R_c) [39-41]. In the case of GRW, the settlement at the backfill reduces uniformly by 20% behind the wall. For the MSE, the effect of

compaction is less along the extent of the geogrid, while the difference outside of this extent can reach up to 50%. The backfill compaction effect is more apparent when looking at the lateral displacement distribution (relative to point A' at the base). As shown in Figure 12b, compacting the backfill from D_r = 70% to 100% reduced the lateral displacement by at least 42% for both GRW and MSE systems, regardless of the excitation.

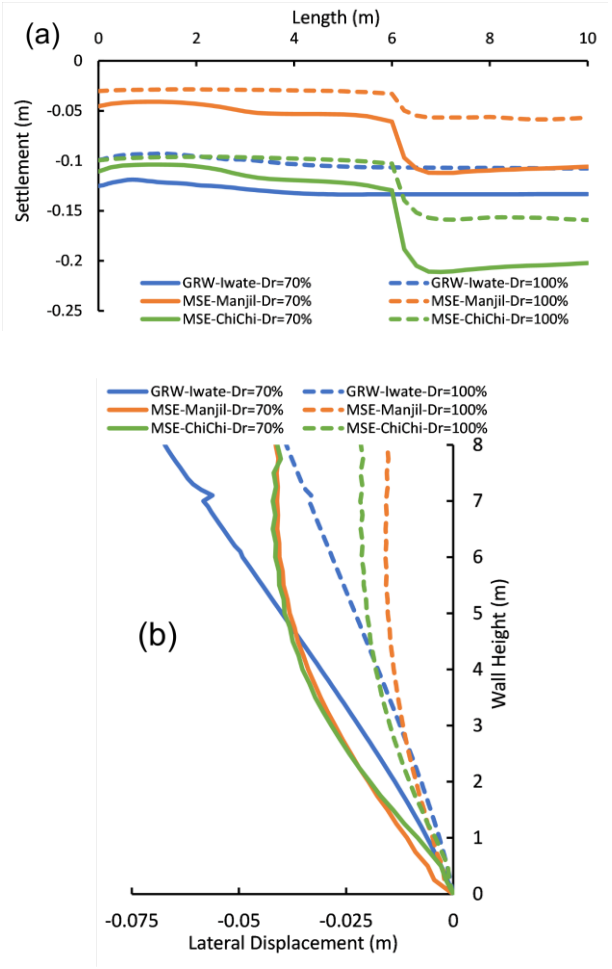

Figure 12: Comparison between backfill soil of D_r = 70%, and 100% for a) Settlement at the backfill top level, and b) lateral displacement distribution of the wall relative to wall base (A').

In the case of the MSE system subjected to the ChiChi motion (Figure 13), both the D_r = 70% and 100% backfills show traits of global failure mechanism (deep-seated). However, the extent of the failure surface might penetrate deeper into the backfill behind the MSE system for D_r = 70% (Figure 13a) compared to D_r = 100% (Figure 13b) for the same seismic demand. Note that the Figure 12b lateral displacements are relative to the base (point A' in Figure 1) and the values in Figure 13 are absolute.

CONCLUDING REMARKS

The primary purpose of this study was to compare the seismic response of mechanically stabilised earth (MSE) structures and gravity cantilever retaining walls (GRW). Through 1D and 2D OpenSees finite element modelling and GiD post-processing, we have studied the behaviour of the mentioned retention systems under three seismic records and a series of sinusoidal excitations. The Manzari and Dafalias constitutive model, a two-surface plasticity model with a non-associative flow rule, has been deployed to simulate granular soil. In the end, we have studied the effect of backfill compaction for both backfill retention systems. The findings of this paper are listed below.

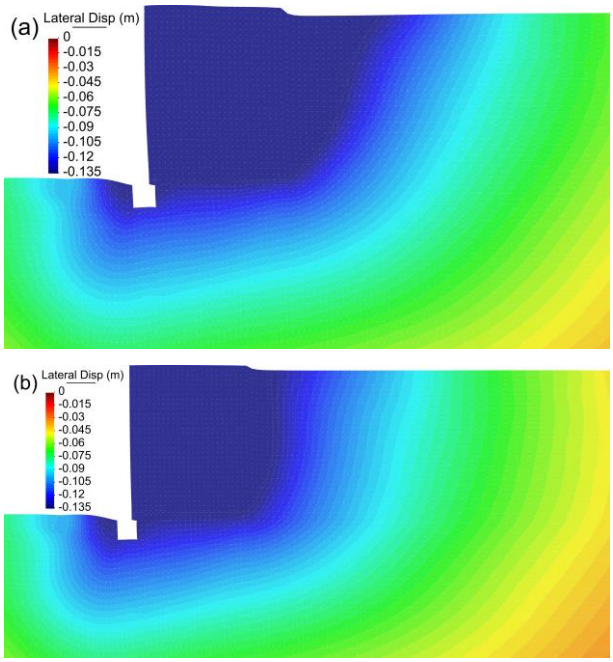

Figure 13: Lateral displacement contours on deformed shape for MSE wall subjected to ChiChi motion when founding soil D_r = 70% and the backfill soil D_r = a) 70%, and b) 100%.

- In this study, 1D site response analyses of an elastic soil column could be a suitable approximation to estimate the natural period of a soil medium with a nonlinear soil column having a 10% longer period (see Figure 4).
- The maximum acceleration response of the 1D linear/nonlinear soil column is almost identical to the wall top in this study 2D linear/nonlinear model. This suggests that the 1D soil column's maximum acceleration can be employed to design the retaining walls. However, this study shows that a 1D elastic soil column can lead to underestimation if used to determine the maximum input acceleration for 2D analyses. For this purpose, a series of 1D site response analyses on nonlinear soil is required (see Figure 4).
- Although for both MSE and GRW systems, the settlement at the bottom of the retention systems is roughly the same, the settlement of the backfill surface is lower for MSE within the extent of geogrid layers. Nevertheless, immediately behind the end of geogrid layers, the backfill surface experienced a sudden increase in the settlement quantity in the case of MSE. This difference in backfill settlement might indicate that geogrid layers work as a confinement system for the retained soil (Figure 6). This sudden drop of settlement can cause damage to any services running behind the MSE wall and should be considered in designing service lines.
- This investigation indicated that the MSE lateral displacement is about half that of the GRW system, with MSE maximum lateral displacement happening below the mid-height of the wall while the maximum is at the top for GRW (Figures 7 and 12b).
- The retained soil in the MSE system behaves close to a rigid block, but this is probably not the case for GRW. The behaviour of the MSE system can resemble a deep-seated or tensional crack at the backfill surface's (global/external) failure mechanism. For the GRW system, the failure

mechanism appears to be internal. Therefore, the assumption that the soil block on top of the foundation heel would behave synonymously with the GRW might not be accurate (Figure 10 and 11).

- When the backfill is compacted from a medium (D_r = 70% or $R_c \approx$ 95%) to a dense state (D_r = 100% or R_c = 100%), the lateral displacement reduces to at least 40% regardless of retention system type in this study (Figure 12).
- It is crucial to note that the mentioned remarks are concluded from the models discussed in this study, and the outcome might vary in different conditions.

ACKNOWLEDGEMENTS

The work of the first-named author was funded by the University of Canterbury Quake Centre (UCQC), the University of Auckland Department of Civil Engineering, and Andy O'Sullivan Geotechnical Engineering. All the analyses have been done through the Mahuika high-speed computing platform of New Zealand e-Science Infrastructure (NeSI). The helpful advice of Dr Christopher McGann and, Dr Alborz Ghofrani and, intellectual inputs of my colleagues Dr Yuri Wong and Dr Romain Meite on aspects of the OpenSees software is much appreciated. Also, the corresponding author expresses his gratitude to his PhD examiners and reviewers, Prof Richard Bathurst, Dr Rolando Orense and, Prof Majid Manzari who helped raising the quality of this work by their comments.

REFERENCES

1 Seed HB and Whitman RV (1970). "Design of earth retaining structures for dynamic loads". *ASCE Specialty Conference on Lateral Stresses in the Ground and Design of Earth Retaining Structures*, Cornell University, Ithaca, New York, pp. 103-147.

2 AASHTO (American Association of State Highway and Transportation Officials). (2020). "*AASHTO LRFD Bridge Design Specifications*". 9th Edition. Washington, DC: AASHTO.

3 Richards JR and Elms DG (1979). "Seismic behavior of gravity retaining walls". *Journal of Geotechnical and Engineering Division*, **105**(4): 449-464. https://doi.org/10.1061/AJGEB6.0000783

4 NZTA (New Zealand Transport Agency). (2013). "*Bridge Manual*", 3rd Edition. NZTA, Wellington, New Zealand.

5 Bathurst RJ and Simac MR (1994). "Geosynthetic reinforced segmental retaining wall structures in North America". *Proceedings of the Fifth International Conference on Geotextiles, Geomembranes and Related Products*, September 5-9, Singapore, 1pp. https://doi.org/10.13140/2.1.4738.8160

6 Stuedlein AW, Allen TM, Holtz RD and Christopher BR (2012). "Assessment of reinforcement strains in very tall mechanically stabilized earth walls". *Journal of Geotechnical and Geoenvironmental Engineering*, **138**(3): 345-356. https://doi.org/10.1061/(ASCE)GT.1943-5606.0000586

7 Leshchinsky D and Vahedifard F (2012). "Impact of toe resistance in reinforced masonry block walls: design dilemma". *Journal of Geotechnical and Geoenvironmental Engineering*, **138**(2): 236-240. https://doi.org/10.1061/(ASCE)GT.1943-5606.0000579

8 Zheng Y and Fox PJ (2016). "Numerical investigation of geosynthetic-reinforced soil bridge abutments under static loading". *Journal of Geotechnical and Geoenvironmental Engineering*, **142**(5): 04016004. https://doi.org/10.1061/(ASCE)GT.1943-5606.0001452

9 Kuwano J, Miyata Y and Koseki J (2014). "Performance of reinforced soil walls during the 2011 Tohoku earthquake". *Geosynthetics International*, **21**(3): 179-196. https://doi.org/10.1680/gein.14.00008

10 Murashev AK (2003). "*Guidelines for Design and Construction of Geosynthetic-Reinforced Soil Structures in New Zealand*". Transfund New Zealand Research Report No. 239, Wellington, New Zealand, 216pp.

11 Kibria G, Hossain MS and Khan MS (2014). "Influence of soil reinforcement on horizontal displacement of MSE wall". *International Journal of Geomechanics*, **14**(1): 130-141. https://doi.org/10.1061/(ASCE)GM.1943-5622.0000297

12 Leshchinsky D and Vulova C (2001). "Numerical investigation of the effects of geosynthetic spacing on failure mechanisms in MSE block walls". *Geosynthetics International*, **8**(4): 343-365. https://doi.org/10.1680/gein.8.0199

13 Safaee AM, Mahboubi A and Noorzad A (2021). "Experimental investigation on the performance of multi-tiered geogrid mechanically stabilized earth (MSE) walls with wrap-around facing subjected to earthquake loading". *Geotextiles and Geomembranes*, **49**(1): 130-145. https://doi.org/10.1016/j.geotexmem.2020.08.008

14 Srivastava A and Chauhan VB (2020). "Numerical studies on two-tiered mse walls under seismic loading". *SN Applied Sciences*, **2**(10): 1-7. https://doi.org/10.1007/s42452-020-03414-6

15 McKenna F, Mazzoni S and Fenves G (2019). "*Open System for Earthquake Engineering Simulation (OpenSees) Software Version 3.1.0*". University of California, Berkeley, CA. Available from http://opensees.berkeley.edu

16 Dafalias YF and Manzari MT (2004). "Simple plasticity sand model accounting for fabric change effects". *Journal of Engineering Mechanics*, **130**(6): 622-634. https://doi.org/10.1061/(ASCE)0733-9399(2004)130:6(622)

17 Coll A, Ribo R, Pasenau M, Escolano E, Perez JS, Melendo A, Monros A and Ga RJ (2016). "*GiD v.13 User Manual* [Computer Software]".

18 Lee KL and Seed HB (1967). "Drained strength characteristics of sands". *Journal of Soil Mechanics and Foundations Division*, **93**(6): 171-141. https://doi.org/10.1061/JSFEAQ.0001048

19 Ghofrani A and Arduino P (2015). "*Manzari Dafalias Material in Opensees*". http://opensees.berkeley.edu/wiki/index.php/Manzari_Dafalias_Material (Accessed March 2020)

20 Jeremić B, Cheng Z, Taiebat M and Dafalias Y (2008). "Numerical simulation of fully saturated porous materials". *International Journal for Numerical and Analytical Methods in Geomechanics*, **32**(13): 1635-1660. https://doi.org/10.1002/nag.687

21 Loukidis D and Salgado R (2011). "Active pressure on gravity walls supporting purely frictional soils". *Canadian Geotechnical Journal*, **49**(1): 78-97. https://doi.org/10.1139/t11-087

22 Sakleshpur VA, Prezzi M and Salgado R (2017). "*Performance Assessment of MSE Aabutment Walls in Indiana*". Joint Transportation Research Program Publication No. FHWA/IN/JTRP-2017/06, West Lafayette, Purdue University. https://doi.org/10.5703/1288284316390

23 Kamalzadeh A and Pender MJ (2019). "Modelling the dynamic response of gravity retaining wall systems using OpenSees". *Earthquake Geotechnical Engineering for Protection and Development of Environment and*

Constructions- Proceedings of the 7th International Conference on Earthquake Geotechnical Engineering, 3161pp. https://doi.org/10.6084/m9.figshare.16571160

24 Ishihara K (2003). *Soil Behaviour in Earthquake Geotechnics*. ISBN: 9780198562245, Clarendon Press, Oxford.

25 Hatami K and Bathurst RJ (2005). "Development and verification of a numerical model for the analysis of geosynthetic-reinforced soil segmental walls under working stress conditions". *Canadian Geotechnical Journal*, **42**(4): 1066-1085. https://doi.org/10.1061/(ASCE)1090-0241(2006)132:6(673)

26 Huang B, Bathurst RJ and Hatami K (2009). "Numerical study of reinforced soil segmental walls using three different constitutive soil models". *Journal of Geotechnical and Geoenvironmental Engineering*, **135**(10): 1486-1498. https://doi.org/10.1061/(ASCE)GT.1943-5606.0000092

27 Mcgann CR, Arduino P and Mackenzie-Helnwein P (2012). "Stabilized single-point 4-node quadrilateral element for dynamic analysis of fluid saturated porous media". *Acta Geotechnica*, **7**(4): 297-311. https://doi.org/10.1007/s11440-012-0168-5

28 Berg RR, Christopher BR and Samtani NC (2009). "Design of mechanically stabilised earth walls and reinforced soil slopes–volume I". *Federal Highway Administration of The United States*, Washington, D.C. https://www.fhwa.dot.gov/engineering/geotech/pubs/nhi10024/

29 Clayton CR, Woods RI, Bond AJ and Milititsky J (2014). *Earth Pressure and Earth-Retaining Structures*. ISBN: 9781466552111, CRC Press.

30 Pender MJ (2017). "Foundation design for gravity retaining walls under earthquake". *Proceedings of the Institution of Civil Engineers-Geotechnical Engineering*, **172**(1): 42-54. https://doi.org/10.1680/jgeen.17.00233

31 McGann C and Arduino P (2015). "*Dynamic 2D Effective Stress Analysis of Slope*". http://opensees.berkeley.edu/wiki/index.php/Dynamic_2D_Effective_Stress_Analysis_of_Slope (Accessed November 2018)

32 Chin CY, Kayser C and Pender MJ (2016). "Seismic earth forces against embedded retaining walls: insights from numerical modelling". *Bulletin of the New Zealand Society for Earthquake Engineering*, **49**(2): 200-210. https://doi.org/10.5459/bnzsee.49.2.200-210

33 Pender MJ and Kamalzadeh A (2019). "Insights from advanced numerical modelling into the pseudo-static design of gravity retaining walls". *Earthquake Geotechnical Engineering for Protection and Development of Environment and Constructions- Proceedings of the 7th International Conference on Earthquake Geotechnical Engineering*, 535pp. https://doi.org/10.6084/m9.figshare.16571169

34 Lysmer J and Kuhlemeyer RL (1969). "Finite dynamic model for infinite media". *Journal of the Engineering Mechanics Division*, **95**(4): 859-878. https://doi.org/10.1061/JMCEA3.0001144

35 Joyner WB and Chen ATF (1975). "Calculation of nonlinear ground response in earthquakes". *Bulletin of the Seismological Society of America*, **65**(5): 1315-1336. https://doi.org/10.1785/BSSA0650051315

36 Kokusho T and Sato K (2008). "Surface-to-base amplification evaluated from Kik-Net vertical array strong motion records". *Soil Dynamics and Earthquake Engineering*, **28**(9): 707-716. https://doi.org/10.1016/j.soildyn.2007.10.016

37 Ancheta TD, Darragh RB, Stewart JP, Seyhan E, Silva WJ, Chiou BS, Wooddell KE, Graves RW, Kottke AR and Boore DM (2013). "*Peer NGA-West2 Database*". https://ngawest2.berkeley.edu/ (Accessed March 2020)

38 Bathurst RJ, Hatami K and Alfaro MC (2021). "*Geosynthetic-reinforced Soil Walls and Slopes – Seismic Aspects*". *Chapter 19 in ICE Handbook of Geosynthetic Engineering*, 371-415. ISBN: 978-0-7277-6500-0, ICE Publishing.

39 Lee KL and Singh A (1971). "Relative density and relative compaction". *Journal of the Soil Mechanics and Foundations Division*. **97**(7): 1049-1052. https://doi.org/10.1061/JSFEAQ.0001642

40 Patra C, Sivakugan N, Das B and Rou S (2010). "Correlations for relative density of clean sand with median grain size and compaction energy". *International Journal of Geotechnical Engineering*, **4**(2): 195-203. https://doi.org/10.3328/IJGE.2010.04.02.195-203

41 Mujtaba H, Farooq K, Sivakugan N and Das B (2020). "Laboratory and field investigations in granular soils to correlate relative density, relative compaction and grain size". *Journal of the South African Institution of Civil Engineering*, **62**(2): 12-21. http://dx.doi.org/10.17159/2309-8775/2020/v62n2a2